17th World Conference on Earthquake Engineering, 17WCEE
Sendai, Japan - September 13th to 18th 2020

RUBBER BEARINGS WITH FLEXIBLE SUPPORTS: IMPLICATIONS FOR ISOLATED BRIDGES

T.C. Becker[1], R.E. Darlington[2], M.C. Lopez Ruiz[3]

[1] *Assistant professor, University of California Berkeley, tcbecker@berkeley.edu*
[2] *Design engineer, Read Jones Christoffersen, Rdarlington@rjc.ca*
[3] *Graduate student University of California Berkeley, camila.lopez@berkeley.edu*

Abstract

Traditionally, in the design of isolation bearings for bridge applications, bearing rotations due to seismic conditions are neglected. This comes from the assumption that boundary conditions are rigid and, as such, the bearing end-plates remain parallel as the bearings shear. However, for bridges with tall piers, the pier flexibility may lead to rotations at the base of the bearings, and flexibility of the bridge deck will lead to rotation at the top of the bearing. Thus, typical assumptions about bearing end conditions may be invalid. Furthermore, there is no guidance on the necessary stiffness of the framing elements to assume typical end conditions. This paper presents experimental studies on the behavior of natural and lead rubber bearings placed at a column top. The subassembly is quasistatically tested with increasingly smaller columns, resulting in rotation at the bottom of the bearings. In combination, increasing rotational demands are applied at the top of the bearing, so that both top and bottom end conditions assumptions are challenged. The experiments find significant decreases in bearing stiffness at the fixed end conditions are relaxed. Additional stability tests were conducted with the natural rubber bearing mounted on top of the columns to compare against numerical bearing stability models that assume parallel end plate conditions or end plates with permanent (static) rotation. The findings from the experimental research are used to evaluate potential changes in performance of a bridge with tall piers. The bridge model is developed in *OpenSees* and analyzed under design and maximum considered earthquake levels to determine the seismic demands on the isolation bearings particularly focusing on the rotational demands. The bearing models are then updated to account for the rotational flexibility and the changes in bridge displacement demands under seismic motion as well as force demands into the piers and deck are evaluated.

Keywords: rubber bearings, tall bridge priers, isolated bridges, boundary conditions

1. Introduction

Traditional applications of isolation assume parallel and unrotated top and bottom end plates. However, there are some situations when the parallel end plate assumption may not be valid. If the building columns or bridge piers below the bearings, or the floor diaphragm or bridge deck above, are not rigid, the bearings may experience rotations at one or both ends of the isolator, potentially affecting isolator design criteria such as bearing buckling and horizontal stiffness, which are largely based on analytical models and experimental tests that do not account for the effects of boundary rotation.

Experimental testing on the horizontal behavior of elastomeric bearings has largely been conducted using parallel end conditions, and thus, design values are typically informed by experimental testing that does not necessarily represent the end conditions in tall bridge piers. However, Ishii et al. [1] investigated the moment-rotational behavior by applying cyclic rotations at pre-applied constant shear strains. They found that bearing rotational stiffness increases with increasing vertical load but decreases with increasing shear strain. In an opposite approach, Rastgoo Moghadam [2] tested a natural rubber bearing (NRB) with a constant single end plate rotation, representative of settlement or installation errors. They concluded these constant rotations can impart initial forces, shifting the hysteretic loops where the magnitude of shift is influenced by axial loads. Chen et al. [3] tested full-scale high damping rubber (HDR) bearings under multiaxial excitation including pitch, roll, and yaw. While the effects of the rotations on horizontal stiffness were less than 5%, the peak rotations were 0.0043 rad, which is representative of typical new building applications [4] where there are rigid diaphragms bounding the isolation system. None of these experiments simulated the combinations of demands that would arise from flexible framing bounding the bearing.

Crowder and Becker [5] considered the horizontal behavior of a column-top elastomeric isolation system with various columns of decreasing stiffness and concluded that flexible boundary conditions can significantly reduce the horizontal stiffness of the bearing. The experimental program which only included NRBs did not consider rotation at the top of the bearing or investigate the effect of axial loading. The experimental program presented in this study explores these gaps using an NRB and a lead rubber bearing (LRB) in a column-isolator system with varied applied top plate rotations under multiple axial loads.

Research on non-seismic elastometric bridge bearings, designed for thermal expansion, has established rotational limits for the bearing so that they can maintain serviceability. However, when deisgning isolated bridges it is typically assumed that the endplates remain parallel [6]. Too investigate the validity and effects of this assumption, the results from the experimental study on column-isolator assemblies are used in conjunction with a model of an existing bridges with isolated piers that increasing in height from 10.7 m to 44.2 m.

2. Experimental tests on NRB and LRB bearings

To assess the effects of top and bottom plate rotation and large shear strain on the horizontal behavior of elastomeric bearings, a quarter-scale experimental program was conducted at McMaster University, Canada. The test setup (Fig.1) had an NRB or LRB bearing at the top of various columns. The setup was modified from Crowder and Becker's [5] which could not apply rotation at the top of the bearing. The column sits on a platform onn linear rails, driven by a displacement controlled horizontal actuator. Two force-controlled vertical actuators connected to the reaction columns were used to apply vertical load to the system through the loading beam. To apply rotation at the top of the bearing, a controlled pinned connection was used with two paired single-acting vertical actuators on either side.

The properties of the bearings tested are in Table 1. While the bearings have similar horizontal stiffness, the LRB is larger and slenderer with almost half the height to width aspect ratio or second shape factor, S2, of the NRB. The theoretical bearing buckling loads presented are based on the overlapped area method of buckling calculations by [7].

Three columns, 0.875 m tall, were tested with each bearing. The two stiffest columns were designed to stay elastic during cyclic testing while the smallest column was designed to yield. The properties of the columns can be found in Table 1. To link the bearing properties to its supporting substructure, the columns are presented in terms of a stiffness ratio (SR) between the horizontal stiffness of the bearing and the column. With flexible column substructures, the stiffness of the column in the bearing-column subassembly is like a cantilever [5]. As a result, the SR is found as

$$SR = \frac{K_{bearing}}{K_{column}} = \frac{\frac{GA}{t_r}}{\frac{3EI}{L^3}} \quad (1)$$

where G is the shear modulus of rubber, A is the area of rubber including cover, and t_r is sum of the thickness of rubber layers. E, I, and L are the Youngs modulus, second moment of area, and length, respectively, of the supporting column. For the LRB, the SR is calculated based on the theoretical secant stiffness of the LRB at 100% shear strain.

The NRB and LRB specimens were tested under cyclic horizontal displacement with proportional rotation at the top of the bearing. Horizontal cycles were gradually increased up to 100 mm (253% shear strain for the NRB and 104% shear strain for the LRB) with two cycles at each displacement increment, as shown in Fig. 2. Rotations were increased proportionally to the displacement, as would be seen under typical first mode behavior or from overturning moment, as seen experimentally in a building tested by Chen et al. [4]. Cyclic rotations of up to 0.01 rad and 0.02 rad were applied for the NRB, while only rotations up to 0.01 rad were usesd for the LRB. All tests were performed at two different axial loads for each bearing. For the NRB, axial loads of 2.5 MPa and 5 MPa corresponding to 50 and 100 kN were used. For the LRB, axial loads of 1.25 and 2 MPa corresponding to 50 and 80 kN were selected. Axial loads and top-plate rotational demands were limited for the LRB because of its low shape factor which leads to low buckling load, and buckling load further decrease with boundary flexibility.

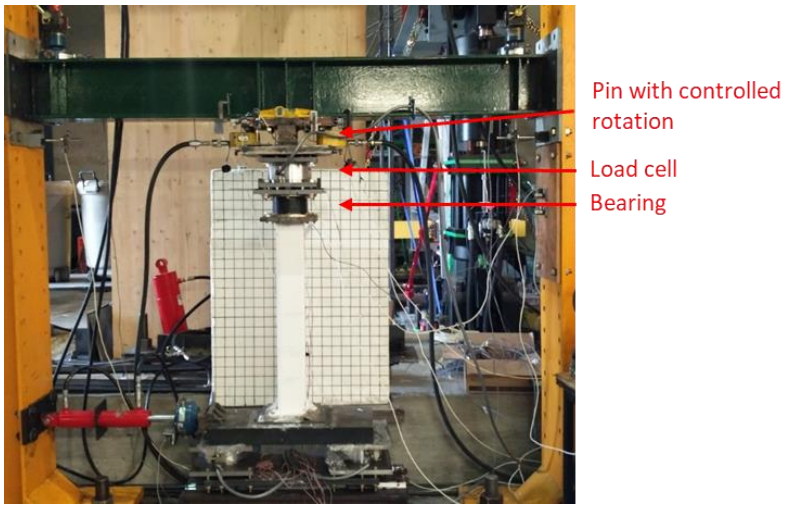

Fig. 1 - Column-top test setup with NRB and HSS127x127x8.0 column

Table 1 - Bearing properties

Bearing Property	**Natural Rubber Bearing (NRB)**	**Lead Rubber Bearing (LRB)**
Radius (mm)	80.0	114.3
Area of rubber (mm2)	20110	39900
Lead core radius (mm)	n/a	19.0
Rubber layer thickness (mm)	1.98	6.0
Steel shim thickness (mm)	1.0	2.7
Total rubber thickness (mm)	39.6	96.0
Height (mm)	101.8	210.0
Shape Factor, S1	19.6	7.9
Shape Factor, S2	4.54	2.38
Shear modulus (MPa)	0.40	0.40
Overlap P_{crit} at 100% strain (kN)	475.4	102.6

Table 2 - Column properties

Column Size	***I* (10^6 mm^4)**	***SR*$_{NRB}$ (%)**	***SR*$_{LRB}$ (%)**
HSS127x127x8.0	7.7	2.9	3.8
HSS102x102x8.0	3.7	6.1	7.8
HSS76x76x4.8	1.0	22.7	29.1

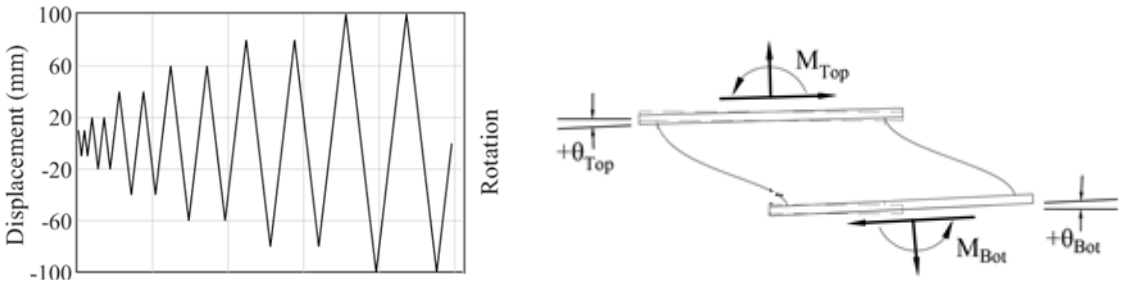

(a) (b)

Fig. 2 - (a) Displacement protocol (b) Bearing positive notation

2.1 Natural rubber bearing assemblies

The shear-displacement measured in the global horizontal axis and the top and bottom moment-rotation responses of the NRB bearing with the three column assemblies are shown in Fig.3 for 5 MPa axial pressure. The global horizontal stiffness of the bearing is impacted by the presence of both top and bottom boundary rotation, θ_{top} and θ_{bot}. The rotation of the top plate of the bearing plate relative to the bearing plate is termed the local rotation, defined as

$$\theta_{local} = \theta_{top} - \theta_{bot} \tag{2}$$

While using θ_{local} to investigate bearing behavior is most intuitive, there is a strong relationship with the total rotation of the bearing, θ_{total}, which is the total rotation applied to the end bearing boundaries shown as

$$\theta_{total} = \theta_{top} + \theta_{bot} \tag{3}$$

If both the top and the bottom of the bearing are rotated 0.02 rad clockwise, θ_{local} is 0 rad while θ_{total} is 0.04 rad. This scenario can be seen in Fig.4(b), where the top plate and bottom plate are equally rotated and represent a parallel, although flexible end condition.

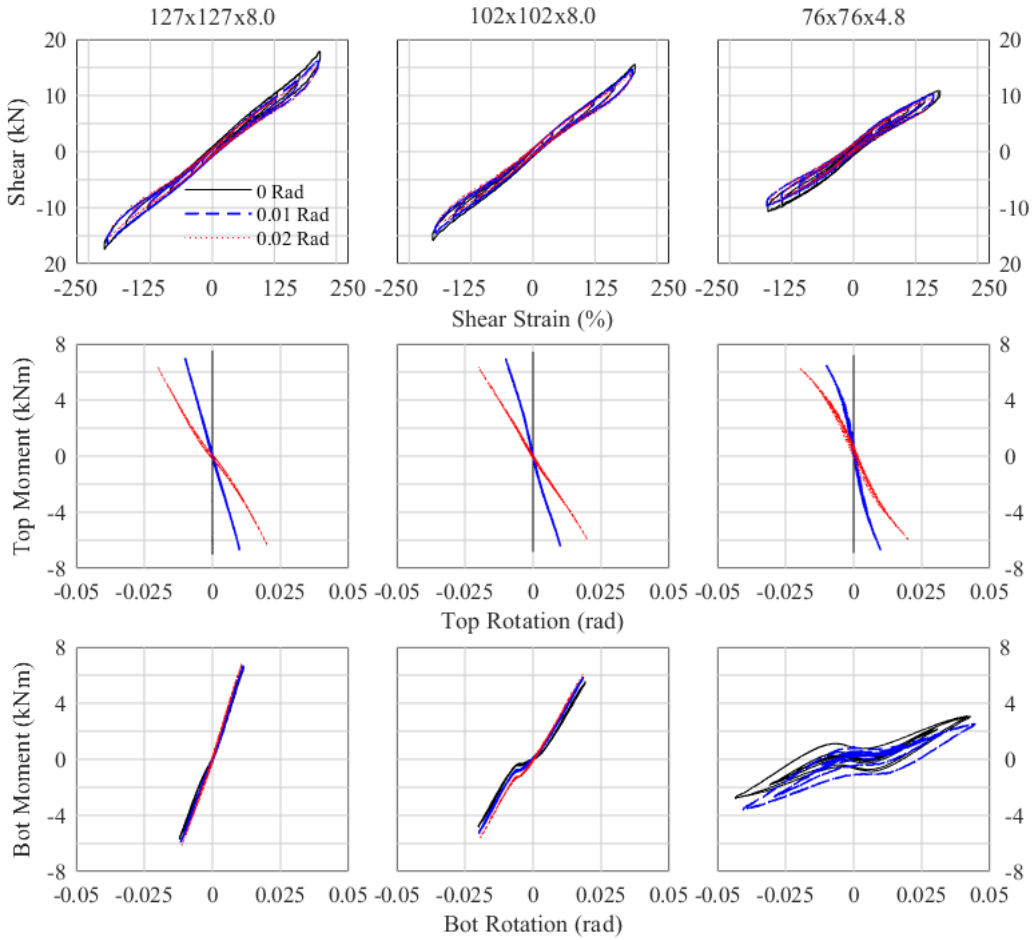

Fig. 3 - Force-displacement, top and bottom moment-rotation responses of column subassemblies at 5 MPa axial load (100 kN)

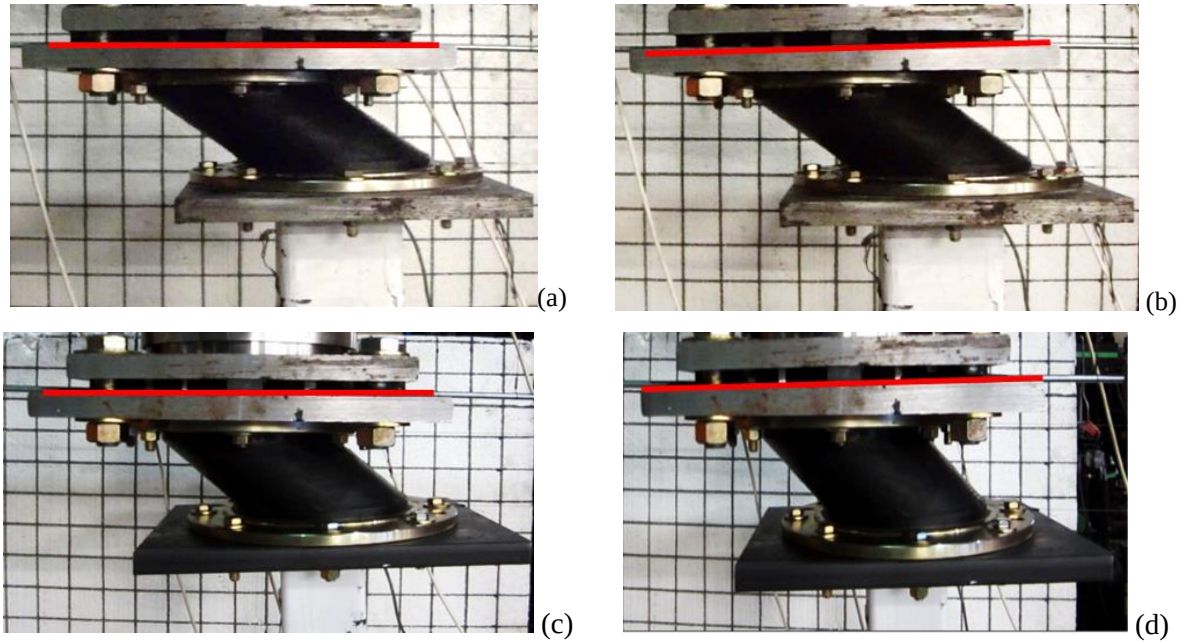

Fig. 4 - (a) NRB-102x102x8.0 with θtop = 0 (b) NRB-102x102x8.0 with θtop = 0.02 rotation, (c) NRB-76x76x4.8 with θtop = 0, (d) NRB-76x76x4.8 with θtop = 0.02

The combination of applied rotation and a flexible supporting column resulted in cumulative decreases in horizontal bearing stiffness of roughly 20%, but this scenario represents an extreme boundary case with a column with a SR of 22.7% (resulting in peak θ_{bot} = 0.045 rad) and applied θ_{top} of 0.02 rad. More realistic design scenarios are represented by the 127x127x8.0 and 102x102x8.0 columns, where decreases in horizontal stiffness of roughly 4% to 13% were observed during the cyclic tests. The reduction in horizontal stiffness due to rotation is roughly 3.5-4.5% per 0.01 rad θ_{total} for 5 MPa and 1.5-2.5% per 0.01 rad θ_{total} for the 2.5 MPa load case, as shown in Fig.5. So, interestingly, the decrease in horizontal stiffness is approximately equal between tests when the θ_{total} is equal, regardless of at which end the rotation is applied. This means that bearing test setups capable of rotating only one end plate can capture the expected decrease in horizontal stiffness by applying the θ_{total} instead of the predicted combination of θ_{top} and θ_{bot}.

Change of horizontal stiffness with pressure is well recognized as a combination of change in shear modulus of the elastomer, G, and P-Δ effects [8]. However, here, even the coupling term with rotation is influenced. As seen in Fig.5, larger axial load level pressure results in a higher decrease dependency of horizontal stiffness on rotation. This trend agrees with the conclusion drawn by Karbaksh Ravari et al. [9] from the Haringx [10] derivation for rotated boundary conditions, where the horizontal stiffness decrease due to rotated boundary conditions is a function of axial loading. A comparison of secant stiffnesses with different end conditions at a range of strains is shown in Fig.6. Application of θ_{top} applied in conjunction with shear unfiromly decreases the shear stiffness over all shear strain levels.

Both the bottom moment and rotation were influenced by the application of rotation at the top of the bearing. While applied top rotation increased the bottom moment, it also decreased the bottom rotation by up to 10%. Thus, while the decreased horizontal stiffness is dependent on θ_{total}, the distribution of bending moment is dependent on the rotation of one plate with respect to the other θ_{local}. This can be seen in the top moment-rotation plot of Fig.3 when the rotation is equal at the top and bottom plate, such as for the 102x102x8.0 column with 0.02 rad of applied rotation. In these essentially parallel boundary conditions, the top and bottom have nearly equal moments. Furthermore, when there is a difference between θ_{top} and θ_{bot}, there is a nonlinear moment-rotation relationship with curvature that changes with the magnitude of θ_{top} relative to θ_{bot}. This moment-rotation relationship is linear when parallel boundary conditions are maintained (θ_{local} = 0 rad).

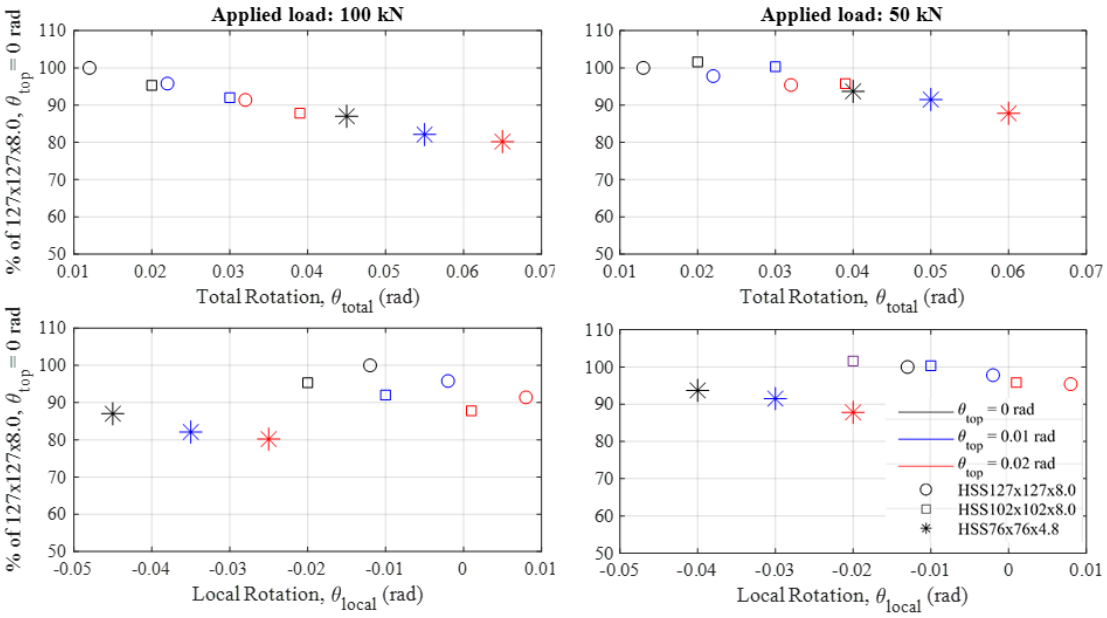

Fig. 5 - Bearing stiffness decrease with total rotation, θ_{total}, and local rotation, θ_{local}, at 100% shear strain and (a) 5 MPa and (b) 2.5 MPa compared against HSS127x127x8.0 with rigid top conditions

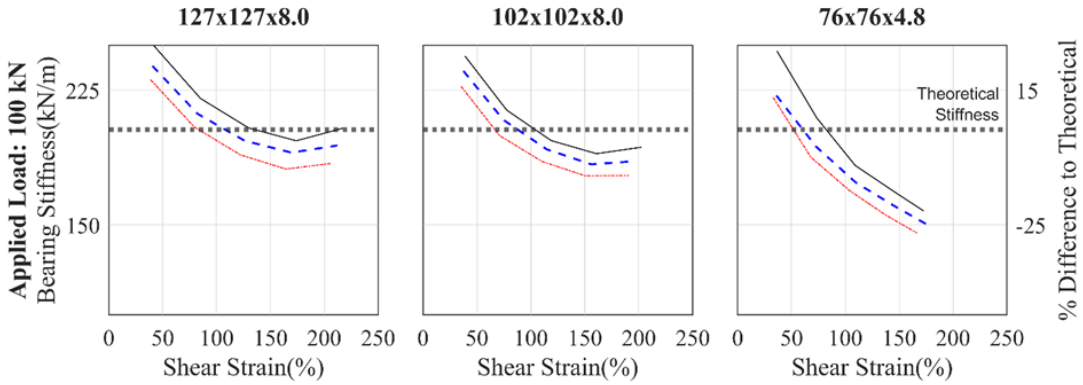

Fig. 6 - Comparison of global NRB stiffnesses with 5 MPa

The NRB was then tested to 300% shear strain under axial loads of 7 to 11 MPa with the two stiffer columns. These axial loads correspond to 96% to 150% of the theoretical overlap buckling load at 300% shear strain. The deformed shape at 300% shear strain is shown in Fig.7. Both columns experienced minor inelastic yielding, but none of the bearing-column subassemblies exhibited negative stiffness. Thus, the simplified overlap method to find the buckling load was suitable for these bearings even under extreme rotations (0.016 rad and 0.029 rad of rotation at the bottom of the bearing for the 127x127x8.0 and 102x102x8.0 subassemblies respectively). This finding is limited to bearings of similar shape factor as bearings with lower shape factors are more susceptible to instability. After these extreme rotations, the bearing was tested to 200% strain under 5 MPa with the stiffest column to compare against the original behavior. The comparison is shown in Fig.8. The one-sided hysteresis loop is nearly identical to that from before large rotations were imposed; however, there is no longer strain hardening at 200% shear strain. This shows excellent resiliency for the bearing under combined shear strain and large rotation.

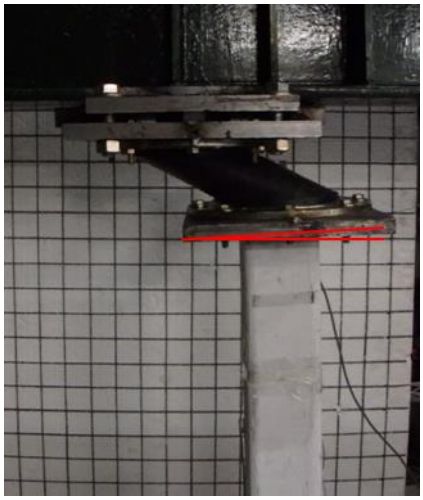

Fig. 7 - NRB tested to 300% shear strain supported by the 102x102x8.0 column, θ_{local} = 0.028 rad.

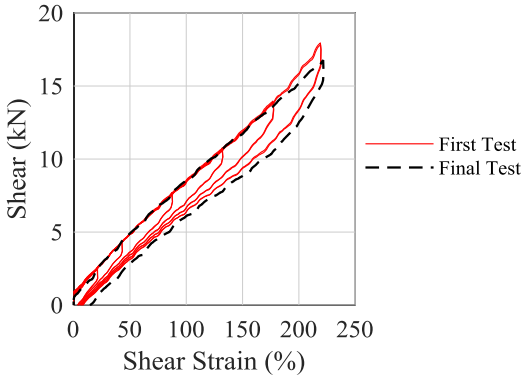

Fig. 8 – NRB behavior pre and post extreme loading scenarios, 5 MPa

2.2 Lead rubber bearing assemblies

The global shear-displacement and top and bottom moment-rotation responses of the lead rubber bearing with the three column assemblies under the range of applied top rotations are shown in Fig.9. There is a pinching behavior, less pronounced in the hysteresis loop for the HSS76x76x8.0 subassembly because of the added hysteretic dissipation from the yielding column. This behavior is caused by a lack of confinement of the lead core due to light axial loads. If lightly loaded, the lead core cannot reach its full yield strength due to vertical slippage of the sides of the lead core or horizontal slippage of the ends of the lead core [11]. A method to increase confinement of the lead core is to decrease rubber layer thickness [12]. As the S1 of the LRB is low (relatively large rubber layer thickness) and was lightly axially loaded, this pinching effect was pronounced.

Similar to the NRB subassemblies, global horizontal stiffness decreases with top and bottom bearing rotation. Under rigid top conditions, the peak bottom plate rotations, θ_{bot}, for the 127x127x8.0, 102x102x8.0, and 76x76x4.8 columns reached 0.017, 0.024, and 0.065 rad of rotation respectively. While the shear strain demands and axial loads are relatively low, these are extremely large rotational demands. The reduction in horizontal stiffness is very similar to the NRB, whith a decrease of roughly 3.5-4.5% per 0.01 rad θ_{total} was observed for both axial pressures.

The 76x76x4.8 presents an extreme boundary condition, where the yielding of the column and bottom rotation of the bearing caused zero tangent stiffness behavior for the 2 MPa load case. This can be seen in the 76x76x4.8 force-displacement plot of Fig. 9, where the tangent stiffness approaches zero. At this shear strain and pressure (55% and 2 MPa), the theoretical buckling load is roughly double (4.2 MPa or 170 kN). Thus,

the flexible boundary conditions have a significant effect on the buckling loads for this bearing with low shape factors (S1 = 4.54, S2 = 2.38). This contrasts against the NRB (S1 = 19.6, S2 = 7.9) conclusions, where the overlap buckling load was conservative.

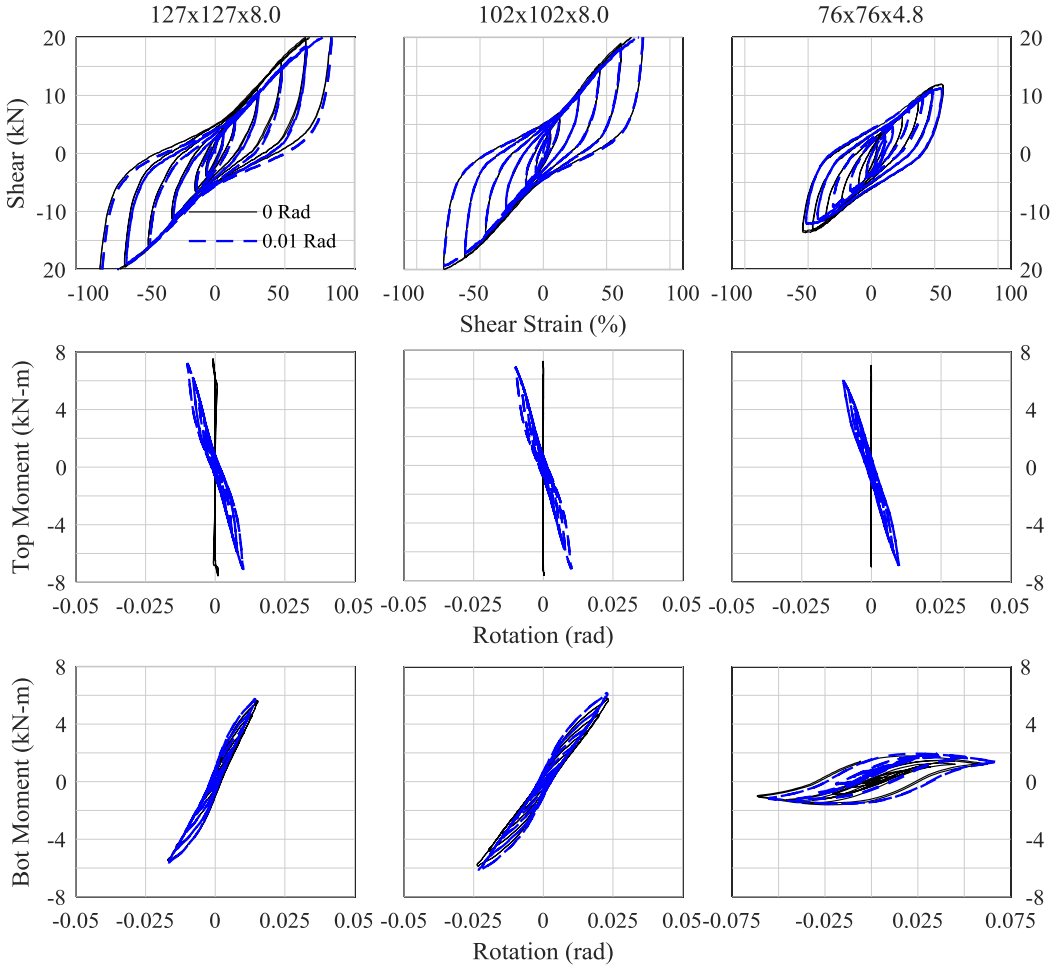

Fig. 9 - Force-displacement, top and bottom moment-rotation responses of column subassemblies at 2 MPa pressure

3. Expected rotations in bridge isolation bearings

3.1 Bridge model

To investigate whether rotations may be a concern for bridges with taller piers, a portion of the Coronado Bridge in California was modled using OpenSees. The bridge sits on rocker bearings at the abutment, on lead rubber bearings on piers 2 through 14, and on pins for the remaining piers. As the bridge is pinned at the abudment and after pier 15, the bridge is not fully isolated in a traditional sense, but the motions of piers 2 through 14 are isolated from the bridge deck motion. The isolated spans are approximately 68 m in length and the piers increase in height from 10.7 m to 44.2 m. Each pier consists of two columns with four isolators placed transverse to the deck on a bent cap. Steel plate girders span from the abutment through pier 18 with steel trusses oriented transverse to the deck. Aditionally, the bridge makes a near 90° bend between piers 4 and 16.

Linear elastic elements are used for all bridge members except for the isolation bearings which were modeled using Bouc-Wen Elastomeric bearing elements. The geometry and details were obtained from 1999 retrofit plans. For simplification of the model, the spans were modeled with stiff elastic beam-column elements, and the trusses were excluded. The abutment was modeled using pinned end conditions. The pier column base nodes were assumed to be fixed, and pier 15 was added with pin connectors between the column cap and the girders using zero-length elements to release the rotations at the top. The first 6 piers of the bridge sit at about a -40° angle from the global x-axis and pier 14 at about a 20° angle from the global x-axis. A modal analysis was preliminarily performed to obtain the natural period of 3.7 s.

Ground motions with 2400 year return period are used in the analysis. This site has stiff soil (180 m/s to 360 m/s) and has resulting short period peudo acceleration of 1.58s and 1 s pseudo acceleration of 0.93. The bridge is right above the Newport-Inglewood-Rose Canyon Fault Zone, about 20 km from the Coronado Bank Fault Zone, and 25 km for the San Diego Through Fault Zone. Eleven acceleration scaled ground motions were obtained using the NGAWest2 library, choosing only motions with magnitudes between 6 and 8 and distances between 0 km and 30 km. The ground motions were scaled to the period of the bridge.

3.1 Predicted responses

The predicted bearing displacement demands are shown in Fig.10. Pier 1 (the abutment) has a rocker bearing and thus no displacement. The bearing demands then increase consistently as the pier height increases. With the increase in displacements comes a larger distribution of demands between the records. However, in general, shear strain demands stayed below 200%. The peak rotations about the two global horizontal directions are shown in Fig.11 for the eleven ground motions, and the rotational orbits for a representative ground motion are shown in Fig.12. There is only a small amount of rotation at the top of the bearing at the deck interface, typically less than 0.005 rad. However, at the bearing-pier interface there are larger rotations that increase in amplitude with pier height. The peak rotations for the taller piers is on the oder of 0.02 to 0.03 rad for the majority of the ground motions. Thus, the effective bearing stiffness can be expected to decrease on the order of 5-10% for these bearings, furthing increasing displacement demands.

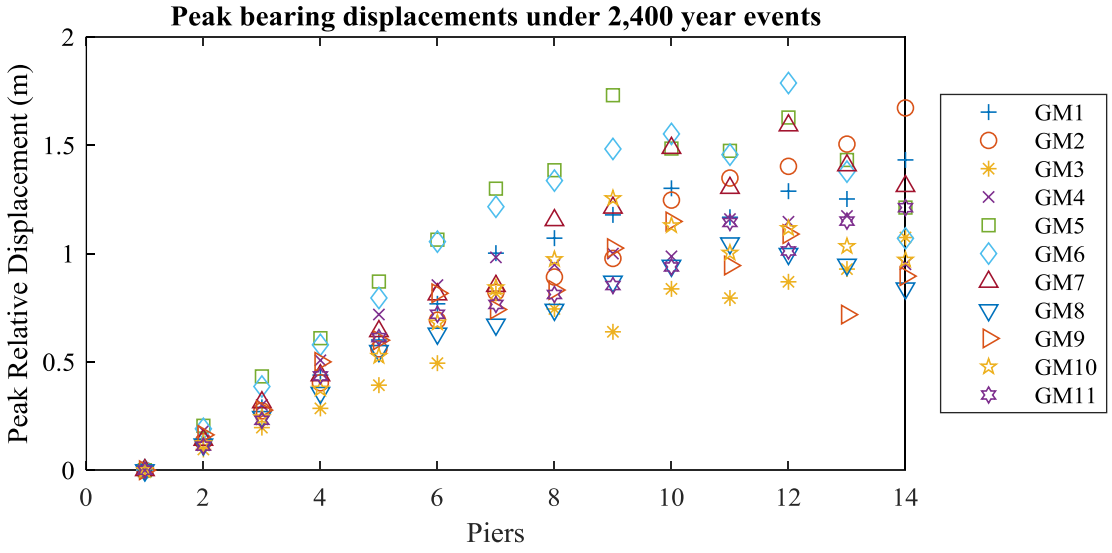

Fig. 10 – Predicted bearing displacement demands

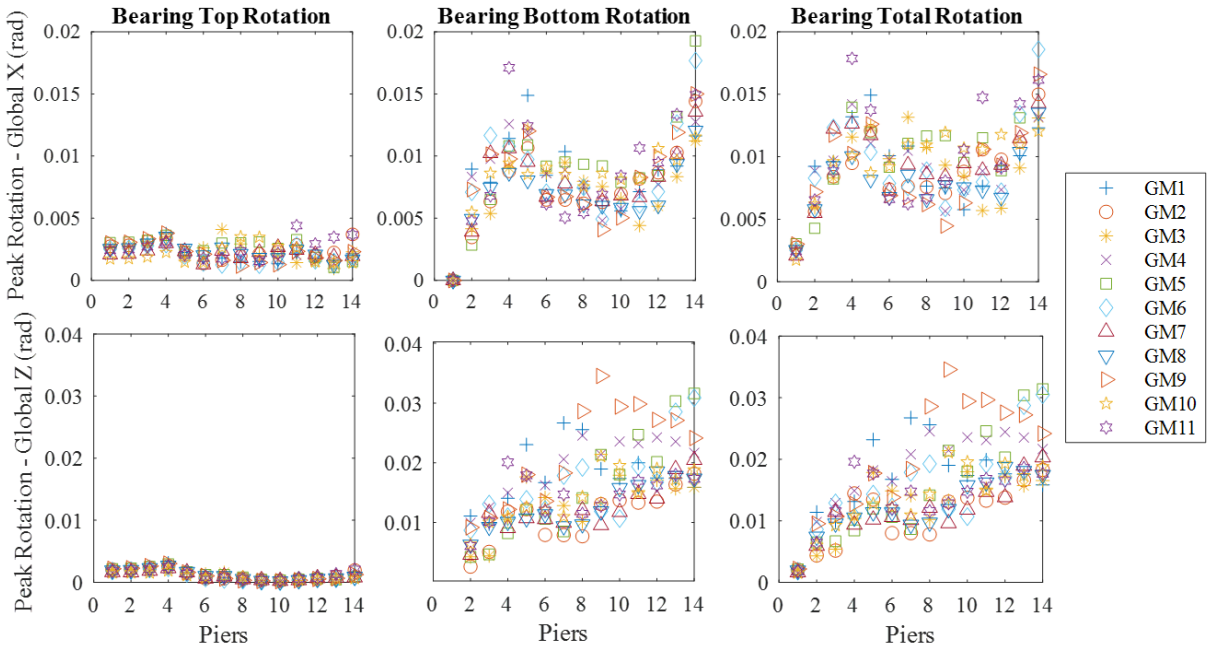

Fig. 11 – Predicted bearing displacement demands

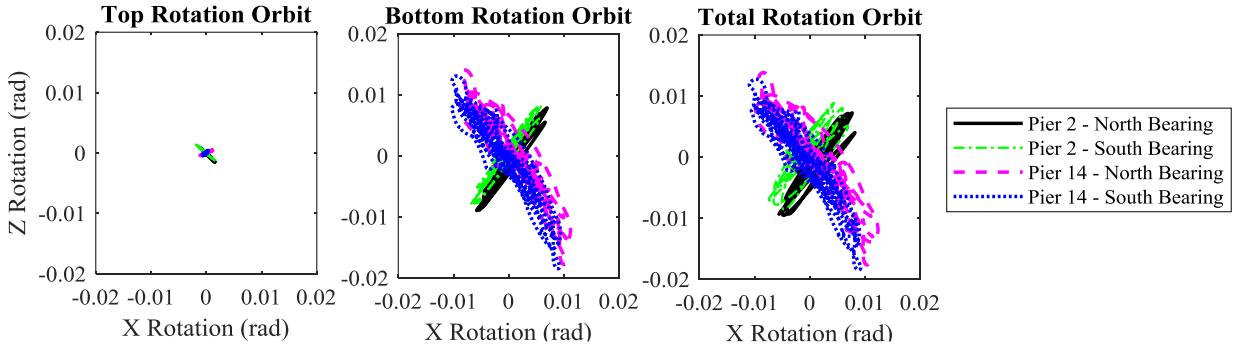

Fig. 12 – Predicted bearing displacement demands for GM4

4. Conclusions

To investigate the potential effects of rotation on pridges with taller piers, an experimental study was conducted in which a bearing-column assembly was tested in which rotation at the top of the bearing was applied simultaneously with horizontal shear. The experiments found that bearing stiffness reduces proportionally to the total rotation of the bearing (rotation of the top plus rotation of the bottom). For the bearing with normal shape factor, stability was maintained under large loads (150% P_{crit} from the overlapping method) and shear strains (300%) even when the bearing is mounted on a moderately flexible column. However, for the bearing tested with very low shape factors, the bearing reached its stability limit well below P_{crit}. As typical isolation bearigns do not have these low shape factors, this should not be a major concern in design. Lastly, the bearing with low shape factors was retested after going through large rotational demands, and the bearing did not show any evidence of damage.

A simplified model of a constructed bridge with increasingly tall isolated piers was then modeled in Opensees. Extrapolating from the experimental data, the bearings in the bridge may expereince decereases in stiffness on the order of 5 to 15%. While small, these reductions in stiffness should be incorporated so that designs accommodate for the increased displacement.

5. Acknowledgements

Financial support for this study was provided by the Natural Sciences and Engineering Research Council (NSERC) Canada.

6. References

[1] Ishii K., Kikuchi M., Nishimura T., Black C.J. (2017). Coupling behavior of shear deformation and end rotation of elastomeric seismic isolation bearings. *Earthquake Engineering & Structural Dynamics*. 46:677–694.

[2] Rastgoo Moghadam, S. (2017). *Effect of support conditions on the behaviour of elastomeric bearings.* (Doctoral Dissertation). McMaster University, Hamilton, Canada.

[3] Chen M, Restrepo JI, Benzoni G (2019): Response of a high damping rubber bearing to multiaxial excitation. *ASTM Journal of Testing and Evaluation.* DOI: 10.1520/JTE20180558

[4] Chen M, Pantoli E, Wang X, Astroza R, Ebrahimian H, Hutchinson T, Conte JP, Restrepo JI, Marin C, Walsh KD, Bachman RE, Hoehler MS, Englekirk R, Faghihi M (2016): Full-Scale Structural and Nonstructural Building System Performance during Earthquakes: Part I – Specimen Description, Test Protocol and Structural Response. *Earthquake Spectra,* **32**(2) 737–770.

[5] Crowder A, Becker T (2017): Investigating substructure flexibility in column-top isolation systems with elastomeric bearings. *Journal of Structural Engineering*, **143**(7).

[6] AASHTO (2014). Guide specifications for seismic isolation design 4th ed. American Association of state and Highway Transportation Officials.

[7] Buckle IG, Liu H (1994): Experimental determination of critical loads of elastomeric bearings at high shear strain. *NCEER Bulletin,* **8**(3), 1-5.

[8] Koh CG, Kelly JM (1987): Effects of Axial Load on Elastomeric Isolation Bearings. *Report UCB/EERC*-86/12, Earthquake Engineering Research Center, University of California: Berkeley, United States.

[9] Karbakhsh Ravari A, Othman IB, Ibrahim ZB, Ab-Malek K (2012): P-Δ and end rotation effects on the influence of mechanical properties of elastomeric isolation bearings. *Journal of Structural Engineering*. **138**(6): 669–675.

[10] Haringx JA (1949): On highly compressible helical springs and rubber rods and their application for vibration-free mountings. III. *Philips Research Reports*. 4: 206-220.

[11] Skinner, R.I., Robinson, W.H., McVerry, G.H. (1993). *An introduction to seismic isolation*, Wiley, New York.

[12] Ryan KL, Kelly JM, Chopra AK (2005): Nonlinear model for lead-rubber bearings including axial-load effects. *Journal of Engineering Mechanics.* 131(12): 1270-1278.

